ELSEVIER

Journal of Power Sources 89 (2000) 7–14

JOURNAL OF POWER SOURCES

www.elsevier.com/locate/jpowsour

Degradation mechanisms in doped spinels of $LiM_{0.05}Mn_{1.95}O_4$ (M = Li, B, Al, Co, and Ni) for Li secondary batteries

Jong H. Lee [a], Jin K. Hong [a], Dong H. Jang [b], Y.-K. Sun [c], Seung M. Oh [a,*]

[a] *Division of Chemical Engineering and Institute of Chemical Process, College of Engineering, Seoul National University, Seoul 151-742, South Korea*
[b] *Finecell, Kyungki-Do 463-070, South Korea*
[c] *Electrochemistry Laboratory, Samsung Advanced Institute of Technology, Daejon 305-380, South Korea*

Received 3 September 1999; accepted 10 December 1999

Abstract

Spinel lithium manganese oxides with a nominal composition of $LiM_{0.05}Mn_{1.95}O_4$ (M = Mn, Li, Al, Co, Ni, or B) are prepared and their degradation mechanisms encountered in lithium secondary cells are investigated. Among the degradation mechanisms proposed in previous reports, those arising either from cation mixing or from the formation of oxygen-deficient spinels are negligible in these materials, but a certain amount of spinel dissolution is observed. X-ray diffraction (XRD) analysis indicates that the spinel lattice experiences an appreciable change in volume during charge–discharge cycling. The extent of this change depends on the nature of dopant. Compared to the undoped spinel, the lattice expansion/contraction according to Li^+ insertion/removal is more significant in the B-doped spinel, but it is smaller in the case of Ni-, Co-, Al-, or Li-doped spinels. Spinels experiencing a smaller volume change maintain their structural integrity, even after prolonged cell cycling, such that there is a better capacity retention. In the B-doped spinel, however, the spinel lattice is largely collapsed and new phases are formed after cell cycling. This results in poor cycleability. It is proposed that the structural breakdown due to the repeated change in lattice volume is the most important failure mode in these materials. Spinel dissolution plays a second major role.

Keywords: Lithium secondary batteries; Lithium manganese oxides; Cathode degradation; Electrochemical voltage spectroscopy; Spinel dissolution

1. Introduction

Spinel lithium manganese oxides, $Li_xMn_2O_4$, are considered to be promising cathode materials for lithium secondary batteries [1–3], but their inferior cycleability, particularly at high temperatures (ca. $> 55°C$), remains a problem [4,5]. Several failure modes have been proposed [6–13] for 4-V $Li_xMn_2O_4$ cathodes. For example, Tarascon et al. [6–8] accounted for the capacity loss by cation mixing between Li and Mn ions in the spinel lattice. The redox peak appearing at 4.5 V (vs. Li/Li^+) has been proposed as an indication of cation mixing. Gao and Dahn [9,10] suggested another failure mode, namely, oxygen loss from the spinel lattice. The discharge plateau appearing at 3.3 V was attributed to oxygen-deficient spinels. The structural breakdown of the spinel lattice, particularly during Li^+ insertion or extraction at the two-phase reaction region ($0.1 < x < 0.4$ in $Li_xMn_2O_4$), has also been proposed to be an important failure mode [11–13].

In previous reports, we have advanced a further failure mode that is deeply related with spinel dissolution [14–16]. This unfavorable reaction takes place mainly at the end of the charging period (at > 4.1 V vs. Li/Li^+), at which potential the solvent molecules in non-aqueous electrolytes are electrochemically oxidized. Acids are generated as a result of the solvent oxidation and the resulting acids promotes dissolution of the spinel. This dissolution induces capacity losses in two ways, viz., material loss from the cathode and polarization loss due to an increase in the electrode resistance. It was also shown that spinel dissolution could be minimized by using electrolytes that are relatively inert to electrochemical oxidation, namely, organic carbonates with fluorine-containing lithium salts (for example, ethylene carbonate/diethyl carbonate/$LiBF_4$ or $LiPF_6$).

Several methods for cycleability improvement of spinel cathodes have been investigated. Among these, the substitution of a small amount of dopant ions at the Mn sites is

* Corresponding author. Tel.: +82-2-880-7074; fax: +82-2-888-1604.
E-mail address: seungoh@plaza.snu.ac.kr (S.M. Oh).

0378-7753/00/$ - see front matter
PII: S0378-7753(00)00375-X

the most commonly quoted [3,4,17–19]. In this case, the basic strategy of doping is, among others, to stabilize the spinel structure against lattice breakdown or Jahn–Teller distortion. Several reports claimed that even if the doping content is small, some quaternary spinel phases $LiM_yMn_{2-y}O_4$ ($y < 0.2$) show better capacity retention than the undoped counterpart. This strategy is, however, in contrast to that of heavy doping, where the primary goal is to exploit new 3 V or 5 V cathode materials [3,20–22]. Some results have shown that the heavily doped spinels $LiM_yMn_{2-y}O_4$ ($y > 0.2$ and M = Ni, Fe, Cr, or Cu) deliver a discharge capacity at 3 V or 5 V at the expense of the capacity at the 4 V region.

This work is an extension of previous studies where the major goal was to improve the spinel cycleability by incorporating a small amount of dopant cations in the spinel lattice. To this end, we have prepared the doped spinels with a nominal composition of $LiM_{0.05}Mn_{1.95}O_4$ (M = Li, B, Al, Co or Ni) and tried to identify the role of dopant cations in determining the cycleability of the spinel. First, a survey was conducted to determine if the above-mentioned failure modes play a major role in doped spinel cathodes. Then, as it was considered that the cycleability improvement by doping may arise from an increase in the electrical conductivity of the doped spinels, the conductivity was measured and correlated to the cycleability data.

2. Experimental

2.1. Materials

Powders of the undoped and doped spinels were prepared by the citrate gel method [23,24]. In this preparation, a stoichiometric mixture of $LiNO_3$, $Mn(NO_3)_2 \cdot 6H_2O$, and H_3BO_3, $Al(NO_3)_3 \cdot 9H_2O$, $Co(NO_3)_2 \cdot 6H_2O$ or $Ni(NO_3)_2 \cdot 6H_2O$ for the nominal composition of $LiM_{0.05}Mn_{1.95}O_4$ (M = Mn, Li, B, Al, Co, or Ni) was dissolved in water with an equivalent amount of citric acid. The resulting aqueous solutions were concentrated to produce sols and then dried in vacuum to give amorphous gels. The gels were then crushed and calcined at 800°C for 8 h. The heating and cooling rate was fixed at 1°C min^{-1}.

To prepare the composite cathodes, the spinel powders were mixed with Ketjenblack ECP-600JD and Teflon binder with a weight ratio of 73:20:7. The mixture was then dispersed in isopropyl alcohol and spread on a piece of stainless steel Exmet (length = 2 mm; width = 1 mm; apparent area = 1 cm^2), followed by pressing and drying at 120°C for 12 h. The electrolyte was 1:1 mixture of EC (ethylene carbonate) and DEC (diethyl carbonate) containing 1 M $LiBF_4$ or 1 M $LiPF_6$ (Tomiyama Pure Chemical). Cell performance was tested in a three-electrode cell, in which lithium foil (Hohsen) was used for the anode and the reference electrode. For the cell capacity to be limited by the cathode such that the observed capacity represents that of the cathodes, an excess amount of lithium metal was used as the anode. In addition, since the dissolved Mn^{2+} ions deposit on the Li anode and reference electrodes, the reference electrode was isolated from the cathode by a Vycor tip, and from the anode by a fritted glass. With this cell configuration, a darkening of the Li electrodes (deposition of Mn on Li electrode surface) can be eliminated, which allows an estimate of the extent of Mn dissolution by an analysis of the electrolyte alone.

For electrical conductivity measurements, pellets of the spinels (diameter = 10 mm; thickness = ca. 1 mm) were prepared by pressing at 20 MPa and sintering at 800°C for 12 h. The density, measured by the Archimedes method, was about 2.6 g cm^{-3}, which amounts to 60% of the theoretical values.

2.2. Instrumentations

Galvanostatic charge–discharge behaviour was analyzed (1 mA cm^{-2}, 0.4 C rate) over a voltage cut-off range of 3.6 to 4.35 V (vs. Li/Li^+). The metal ion contents in the spinel powders were analyzed by an ICP (inductively coupled plasma) technique. The Mn contents and average Mn valence were determined by a potentiometric titration method [25,26]. The oxygen content was then calculated based on the metal ion contents and Mn valence. The dissolved Mn^{2+} concentration in the electrolytes was analyzed by differential pulse polarography. For this, an EG&G PARC Model 174A polarographic analyzer and a Model 303 SMDE were utilized. A tartaric acid/ammonium hydroxide buffer (pH = 9.0) was employed as the electrolyte.

For EVS (electrochemical voltage spectroscopy) measurements, an EG&G PARC M362 potentiostat and a programmable voltage source were combined to control the applied voltage step (= 0.01 V), and the current was continuously monitored until it decayed to a pre-set threshold value ($I_{threshold}$ = 0.02 mA).

The conductivity measurements were made by means of a direct-current method using the van der Pauw configuration [27]. For this, an EG&G PARC M362 potentiostat was utilized as the current source and the voltage was monitored with a digital multimeter (Keithley 2001). The electrical conductivity was measured as a function of temperature in the range 30°C to 90°C.

3. Results and discussion

3.1. Chemical composition and cycling performance of spinel cathodes

The chemical composition and average Mn valence of the spinel materials are listed in Table 1. The chemical

Table 1
Chemical formula and theoretical capacity of undoped and doped spinels

Dopant	Chemical formula	Li %	Mn %	Average oxidation state of Mn	Theoretical capacity[a] (mA h g^{-1})
Li	$Li_{1.02}Mn_{1.96}O_4$	3.99	60.6	3.56	128
B	$Li_{1.00}B_{0.04}Mn_{1.96}O_4$	3.82	59.3	3.51	143
Al	$Li_{0.95}Al_{0.05}Mn_{1.96}O_4$	3.68	60.0	3.52	142
Co	$Li_{0.98}Co_{0.05}Mn_{1.94}O_4$	3.73	58.6	3.54	141
Ni	$Li_{0.99}Ni_{0.05}Mn_{1.94}O_4$	3.75	58.3	3.56	133
None	$Li_{0.98}Mn_{2.00}O_4$	3.75	60.8	3.51	148

[a] Based on a one-electron charge–discharge reaction.

composition of each sample was close to the targetted formula of $LiM_{0.05}Mn_{1.95}O_4$. The slight Li-deficiency in some samples is probably due to Li evaporation during the high-temperature preparation. From the chemical formula, the theoretical capacities based on a one-electron charge–discharge reaction were calculated to be in the range 128 to 148 mA h g^{-1}.

The change in discharge capacity (discharge capacity/initial discharge capacity) is shown in Fig. 1. This was obtained with the spinel cathodes at a current density of 1 mA cm^{-2}. The initial discharge capacity is indicated in the inset. It is apparent that the discharge capacity of the B-doped spinel decreases much faster than that of the undoped one. By contrast, the other doped spinels largely retain their initial capacities for many cycles. For example, the capacity loss observed with the undoped spinel is about 16% after 100 cycles, whereas that for the B-doped and Ni-doped spinel is about 44% and 2%, respectively.

Typical charge–discharge potential profiles are displayed in Fig. 2 for the undoped, Ni-doped and B-doped spinels. The top curves correspond to the charging profiles and the bottom ones to the discharging profiles. Only the 1st, 25th and 100th profiles are presented. Note that the Ni-doped spinel outperforms the others and the B-doped spinel exhibits the poorest behaviour. A comparison of the 1st charge–discharge profiles of the three cathodes reveals that the potential difference between the charging and discharging curve is largest in the B-doped spinel cathode. This suggests that the cell polarization is most serious in this electrode.

Cell polarization arises from various sources, e.g., charge transfer resistance, electrode resistance, and mass-transfer resistance through the electrode materials. In order to assess the relative importance of the electrode resistance, the electrical conductivity of the spinel materials was measured. As can be seen in Fig. 3, the conductivity of the Ni-doped spinel is higher than that of the undoped

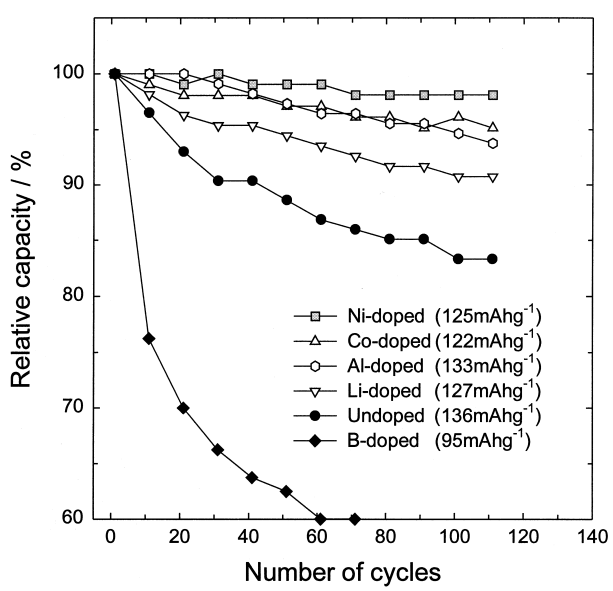

Fig. 1. Change of discharge capacity (discharge capacity/initial capacity) observed with Li/1 M $LiBF_4$ in EC:DEC (1:1 v/o)/spinel cells according to cycle number. The cells were cathode-limited. Galvanostatic cycling was carried out at 1 mA cm^{-2} (0.4 C) between 4.35 and 3.6 V. Cathodes were composed of spinel oxide, Ketjenblack ECP-600JD, and PTFE binder (73:20:7 in wt. ratio). Initial discharge capacity of each spinel cathode is indicated in inset.

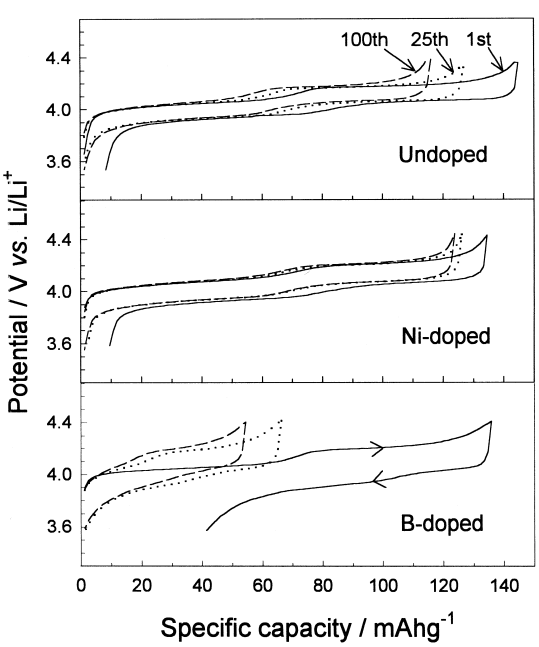

Fig. 2. Galvanostatic charge–discharge potential profiles traced with Li/1 M $LiBF_4$ in EC:DEC (1:1 v/o)/spinel cells. In each profile, upper curves correspond to charging and bottom to discharging. Only those traced at the 1st, 25th and 100th cycles are shown.

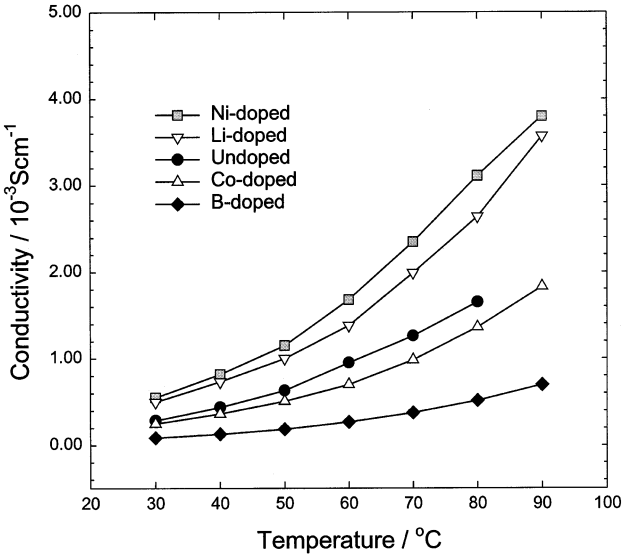

Fig. 3. Electrical conductivity of spinel materials as a function of temperature. Conductivity values were observed at 30°C and activation energy for electrical conduction are listed in Table 2.

one, but the B-doped spinel displays the lowest conductivity. Apparently, there is a relation between the conductivity of electrode materials and the cathode cycleability (Fig. 1); the highest electrical conductivity and best cycleability is found with the Ni-doped spinel, but the lowest conductivity and poorest cycleability is given by the B-doped spinel electrode. A similar relationship between the electrode conductivity and cathode cycleability has been reported in the literature. For example, Tukamoto and West [28] reported that the Mg-doped cobalt oxide $LiMg_{0.05}Co_{0.95}O_2$ is three orders of magnitude higher in conductivity than the undoped counterpart and its cathode cycleability is superior to the undoped one. In the studies reported here, even if there exists a relation between electrical conductivity and cathode cycleability, the conductivity increase obtained on doping is just twice or less at 30°C (Table 2). It is thus difficult to conclude that the electrical conductivity, and therefore the cell polarization, has a crucial effect on the cathode rechargeability in these materials (see Figs. 1 and 3).

Table 2
Electrical conductivity and activation energy for electrical conduction

Dopant	Electrical conductivity[a] (mS cm^{-1})	Activation energy[b] (eV)
Ni	0.55 ± 0.01	0.34 ± 0.01
Li	0.50 ± 0.01	0.34 ± 0.01
Co	0.25 ± 0.01	0.34 ± 0.01
B	0.09 ± 0.01	0.36 ± 0.01
None	0.29 ± 0.01	0.35 ± 0.01

[a] Measured at 30°C.
[b] Determined at 303 to 363 K.

The electrical conductivity observed at 30°C and the activation energy for electrical conduction is listed in Table 2. The conductivity of undoped spinel is 0.29 mS cm^{-1} at 30°C, which is close to the reported value [29]. There is a negligible difference between the activation energy values of the spinel samples. This suggests that the small amount of doping does not perturb the conduction processes in spinel materials.

3.2. Failure modes in spinel cathodes

In order to explain the capacity fading observed with the spinel cathodes (Fig. 1), an assessment has been made of the relevance of the degradation mechanisms proposed in previous investigations of these cathodes. An EVS profile taken for the undoped spinel is given in Fig. 4. As seen, there appears neither the 3.3 V peak nor the 4.5 V redox peak. The absence of these peaks was also confirmed for the other doped spinels. It is clear, therefore, that both cation mixing and oxygen deficiency is negligible in the spinel samples prepared in this study.

The concentration of Mn^{2+} ions in the EC/DEC/1 M $LiBF_4$ electrolyte is shown in Fig. 5(a). This concentration was monitored by differential pulse polarographic analysis of the intermittently sampled electrolyte with cell cycling. The material loss from the cathodes was calculated based on the Mn^{2+} content in the electrolytes, and the fraction of material loss with respect to the total is plotted in Fig. 5(b). As seen, the extent of spinel dissolution from the B-doped spinel is much smaller than that from the undoped or Ni-doped ones. Furthermore, the fractional capacity loss arising from spinel dissolution amounts to less than 10% in the B-doped spinel and ~30% in the undoped and Ni-doped spinel. It is thus very likely that the spinel dissolution itself cannot explain the observed capacity loss.

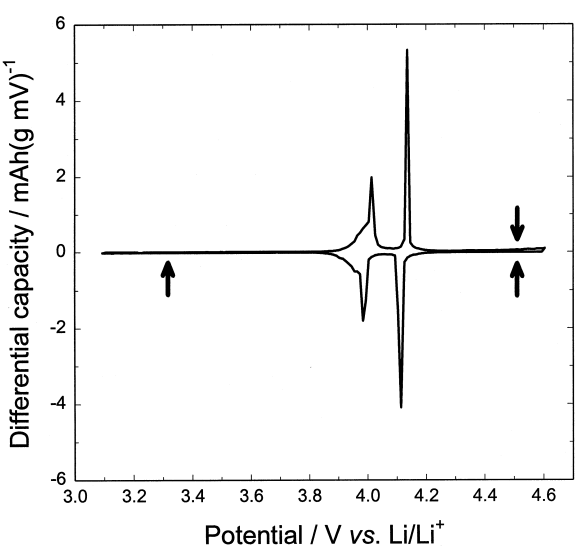

Fig. 4. EVS differential capacity plot traced with undoped spinel. Note absence of peaks at 3.3 and 4.5 V. Other spinels give similar results.

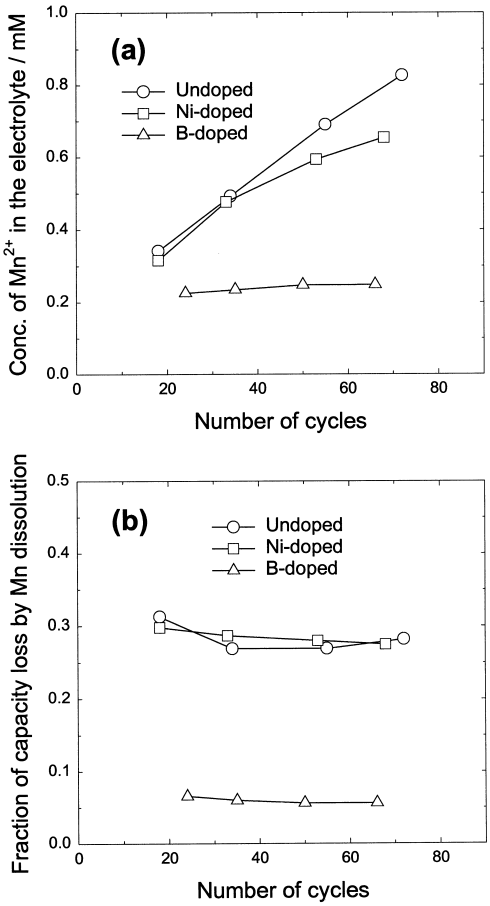

Fig. 5. (a) Concentration of Mn^{2+} ions dissolved from spinel cathodes during charge–discharge cycling; (b) factional capacity loss arising from spinel dissolution. Cathode composition and cycling conditions are the same as for Fig. 1.

3.3. Structural variation according to depth-of-charge

X-ray diffraction (XRD) analysis on the spinel powders indicated that the materials have a spinel structure without discernible impurities. A typical powder XRD pattern is shown in Fig. 8(a). The lattice constants of the spinels (a_o at the fully lithiated state, $x = 1.0$) were calculated from the diffraction data and are listed in Table 3. It is noted that the doped spinels have a smaller (Li-, Al-, Co-, and Ni-doped) or larger (B-doped) lattice constant than the undoped one. Interestingly, the former group outperforms the undoped one, but the latter (B-doped spinel) exhibit poorer behavior. This feature will be discussed later after providing the results on the lattice volume change according to Li^+ insertion/removal.

Table 3
Lattice constant (a_o) at fully lithiated state and rate of change ($\Delta a_o / \Delta x$) with Li^+ removal

Dopant	Lattice constant ($x = 1$) (Å)	$\Delta a_o / \Delta x$	Capacity loss[a] (%)
Ni	8.238	0.131	2
Co	8.235	0.137	5
Al	8.238	0.138	5
Li	8.229	0.142	9
B	8.256	0.193	44
None	8.244	0.170	16

[a] Calculated after 100 cycles.

In general, the topotactic insertion/removal of lithium ions into/from electrode materials is accompanied by a change in the lattice volume, and sometimes by a structural breakdown or transformation to other stable phases. In this study, XRD analysis was performed to examine the change in spinel structure. For this, the spinel cathodes were charged (Li^+ ions are removed) to various pre-set depths (x in $Li_xMn_2O_4$) and then the XRD patterns were obtained. Fig. 6(a) shows the XRD patterns for the undoped spinel. As displayed, removal of Li^+ ions from the spinel framework brings about a shift in the peak to higher angles and a peak splitting at $x < 0.2$. For instance, the $x = 0.2$

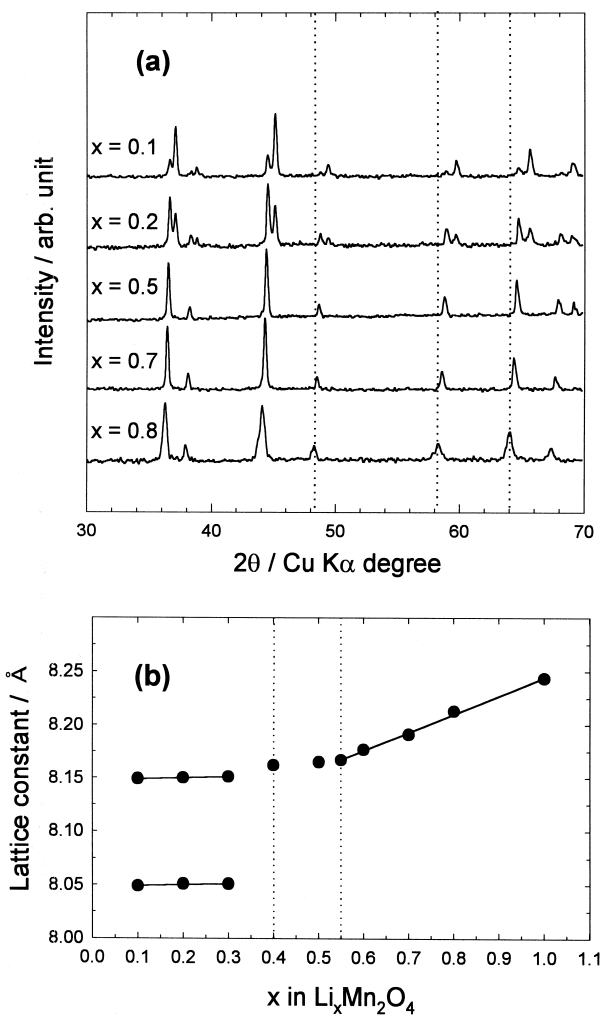

Fig. 6. (a) X-ray powder diffraction patterns for $Li_xMn_2O_4$ as a function of depth-of-charge; (b) change of lattice constant (a_o) with x during first charging. Si powder was used as internal standard, but its peaks are removed for clarity. Note, peak shift and peak splitting at $x < 0.2$ in (a), and lattice contraction with Li^+ removal in (b).

spinel shows a peak splitting at $2\theta = 37°$, 45°, 59°, and 65°, and these peaks move to higher angles. The change in lattice constant (a_o) as a function of x is plotted in Fig. 6(b), where it is seen that the a_o value decreases linearly from 8.244 to 8.167 Å in the region of $0.55 < x < 1.0$, and then remains at a constant value in the range of $0.4 < x < 0.55$. Finally, the peaks are split into two at $x = 0.2$, which indicates that two different cubic phases exist in this region ($x < 0.3$). Similar results have been reported by Xia and Yoshio [11].

X-ray analysis made with the Ni-doped spinel are presented in Fig. 7. Like the undoped one, the diffraction lines gradually move to higher angles with charging. But there appears no peak splitting over the entire region ($0.2 < x < 1.0$), which indicates that a single spinel phase persists over the entire region. The calculated a_o value is plotted against the depth-of-charge in Fig. 7(b), where a monotonic decrease in the lattice constant from 8.238 to 8.137 Å is noticed. The lattice contraction with Li^+ removal is readily explained by an increase in Mn valence with charging. Similar XRD measurements were made with the other doped spinels, for which a gradual decrease in the a_o values without peak splitting is observed. The lattice contraction observed with the B-doped spinel is also presented in Fig. 7(b). Note the difference in the slopes ($\Delta a_o/\Delta x$) between two spinels. A comparison of Figs. 6 and 7 reveals that the phase transition evolving at $x < 0.3$ in the undoped spinel is greatly suppressed by doping. In this sense, considering Yoshio's suggestion [11–13], whereby the spinel framework is collapsed due to the lattice stress imposed by the phase transition occurring at $x < 0.3$, the better cycleability of the doped spinels may be explained by the absence of a phase transition. The observation that the B-doped spinel suffers the most serious capacity losses even without the phase transition encourages a search for other, more tenable, failure modes.

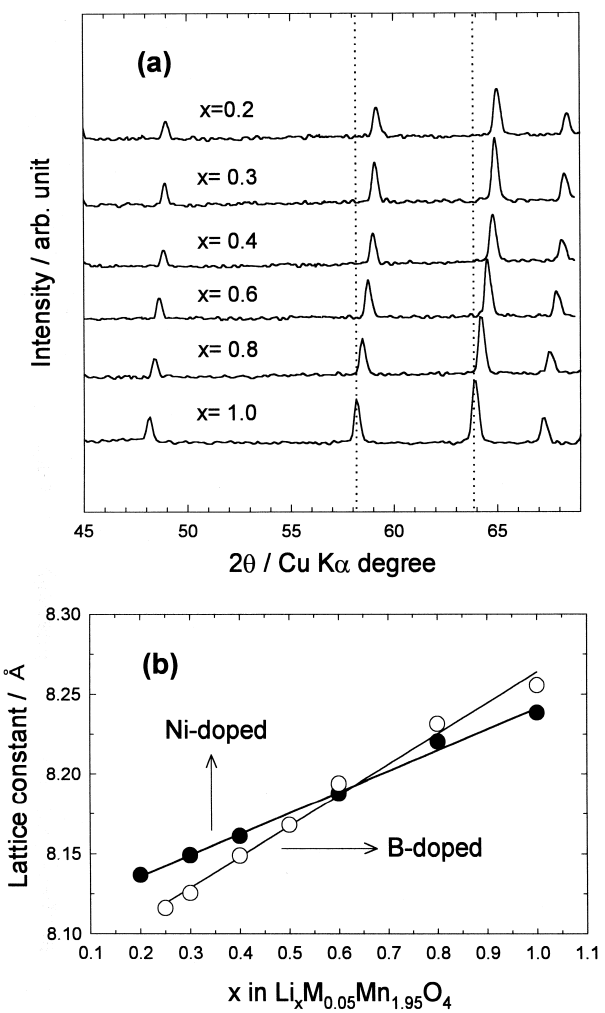

Fig. 7. (a) X-ray powder diffraction patterns of Ni-doped spinel at different depths-of-charge; (b) change of lattice constant (a_o) observed with Ni- and B-doped spinels as a function of x during first charging. Note, diffraction peaks move to higher angles but without peak splitting. Note also the difference in slopes ($\Delta a_o/\Delta x$) between two spinels. Lattice constant at fully discharge state ($x = 1.0$) for other spinels and their changing rate are listed in Table 3.

The change of unit cell constant according to Li^+ ion extraction is listed in Table 3 along with the rate of capacity fading. The percentage capacity loss was calculated from the results obtained after 100 cycles. As already noted, doped spinel has either a smaller or a larger lattice constant than the undoped one. The former group (Ni-, Co-, Al-, and Li-doped spinels) exhibits smaller change in volume ($\Delta a_o/\Delta x = 0.13$–$0.14$) than the undoped spinel ($\Delta a_o/\Delta x = 0.17$). Here, it is interesting to note that these doped spinels show a better cycle performance than the undoped one, but that the B-doped spinel, which suffers the most significant volume change ($\Delta a_o/\Delta x = 0.193$) exhibits the worst capacity retention. Obviously, there exists a relationship between three parameters, namely, the size of the spinel lattice at the fully lithiated state, lattice volume contraction with Li^+ removal, and the rate of capacity fading. Namely, the spinels with a smaller lattice are more resistant against the volume change, which eventually gives rise to a better cycling performance.

3.4. Structural change with extended cell cycling

In order to address the effect that the lattice volume change has on the spinel framework, the spinel cathodes (Ni-, B-doped and undoped ones) were X-ray analyzed with cell cycling (Fig. 8). The XRD pattern of the B-doped spinel in a fresh state is presented in Fig. 8(a). As fresh samples of the other spinels show a similar profiles, they were omitted. The XRD pattern presented in Fig. 8(b) belongs to the Ni-doped spinel, where it is noted that neither impurity phases nor the peak broadening is observed, even after 200 cycles. Thus, the structural integrity is well-maintained. The XRD patterns obtained for B-doped spinel after 1, 100, and 200 cycles are presented in Fig. 8(c) to (e), respectively. Note that the peak intensity

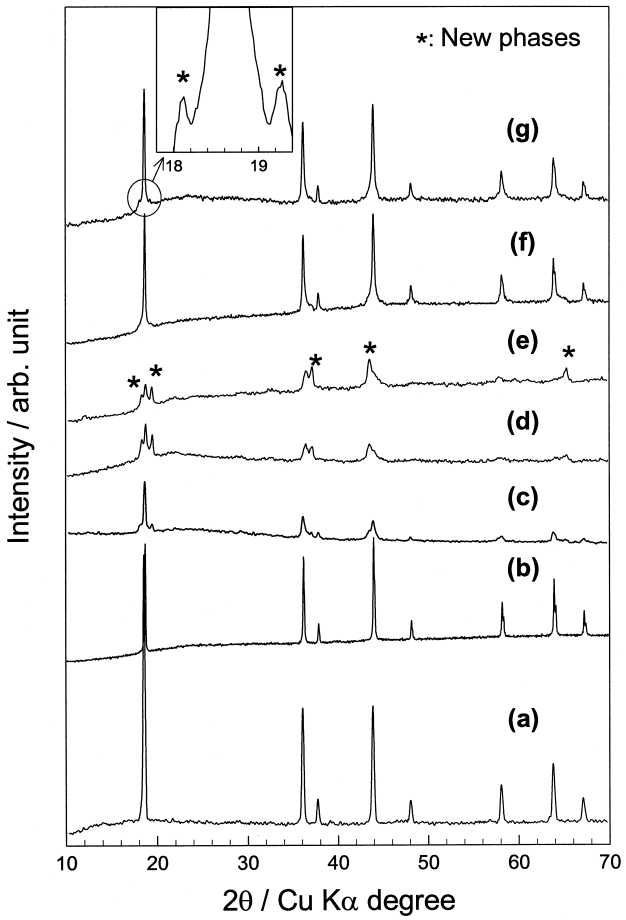

Fig. 8. X-ray powder diffraction patterns for spinel cathodes with cell cycling: (a) B-doped spinel in fresh state; (b) Ni-doped spinel after 200 cycles; (c) B-doped spinel after 1 cycles; (d) B-doped spinel after 100 cycles; (e) B-doped spinel after 200 cycles; (f) undoped spinel after 200 cycles; (g) undoped spinel after 300 cycles.

is greatly reduced and that new peaks develop (marked with *), which shows that the spinel framework is largely collapsed and new phases form. The top two patterns were recorded with the undoped spinel after 200 and 300 cycles, respectively. In this case, the peaks are broader than those observed in the fresh state (as for Fig. 8(a)) and the new peaks are detected at $2\theta = 18°$ and 36°. The new peaks for both the undoped (see the inset) and B-doped spinel are at the same positions, which is indicative of the formation of the same phases from both spinels. Liu et al. [30] reported the formation of tetragonal $Li_2Mn_2O_4$ phases from the undoped and Co-doped spinel after cell cycling. Up to now, the new phases are not characterized, but the diffraction pattern is markedly different from that of the Jahn–Teller distorted tetragonal phases [31].

4. Conclusions

In this work, undoped and doped spinels with a nominal composition of $LiM_{0.05}Mn_{1.95}O_4$ (M = Mn, Li, Al, Co, Ni, and B) have been prepared, and their cathodic properties and failure modes have been examined. The following observations are made.

(i) There appears to be a relationship between the electrical conductivity of spinels and their cathode cycleability, but the conductivity difference between the spinels is too small to be a key determinant of cathode cycleability.

(ii) There is neither the 3.3 V peak nor the 4.5 V redox peak in the EVS profiles of the spinel cathodes; this suggests that all the spinel materials prepared in this work are free from cation mixing and oxygen deficiency.

(iii) The spinel dissolution accounts for $< 30\%$ of the capacity loss, therefore this seems to be only a minor influence on cathode cycleability.

(iv) Li-, Al-, Co-, and Ni-doped spinels have, in their fully lithiated states, a smaller lattice than the undoped one, and they experience a lesser degree of volume change with cell cycling. By contrast, the B-doped spinel has a larger lattice in the lithiated state and shows a substantial change in lattice volume. A lattice breakdown and new phase formation is observed in the B-doped spinel, but the structural integrity of the other doped spinels is largely maintained even after a prolonged cycling. The spinels that experience a smaller volume change give a better cathode cycleability. Breakdown of the spinel framework due to repeated lattice contraction/expansion appears to be an important failure mode in the spinel electrodes.

Acknowledgements

This study was supported by Korean Ministry of Education through Research Fund.

References

[1] J. Desilvesrto, O. Haas, J. Electrochem. Soc. 137 (1990) 5C.
[2] S. Megahed, B. Scrosati, J. Power Sources 51 (1994) 79.
[3] C. Sigala, D. Guyomard, A. Vebaere, Y. Piffard, M. Tournoux, Solid State Ionics 81 (1995) 167.
[4] R.J. Gummow, A. de Kock, M.M. Thackeray, Solid State Ionics 69 (1994) 59.
[5] G.G. Amatucci, C.N. Schmutz, A. Blyr, C. Sigala, A.S. Gozdz, D. Larcher, J.M. Tarascon, J. Power Sources 69 (1997) 11.
[6] J.M. Tarascon, W.R. Mckinnon, F. Coowar, T.N. Bowmer, G. Amatucci, D. Guyomard, J. Electrochem. Soc. 141 (1994) 1421.
[7] J.M. Tarascon, F. Coowar, G. Amatucci, F.K. Shokoohi, D. Guyomard, J. Power Sources 54 (1995) 103.
[8] D. Guyomard, J.M. Tarascon, Solid State Ionics 69 (1994) 222.
[9] Y. Gao, J.R. Dahn, Solid State Ionics 84 (1996) 33.
[10] Y. Gao, J.R. Dahn, J. Electrochem. Soc. 143 (1996) 100.
[11] Y. Xia, M. Yoshio, J. Electrochem. Soc. 143 (1996) 825.
[12] Y. Xia, H. Noguchi, M. Yoshio, J. Solid State Chem. 119 (1995) 216.
[13] Y. Xia, M. Yoshio, J. Power Sources 57 (1995) 125.
[14] D.H. Jang, Y.J. Shin, S.M. Oh, J. Electrochem. Soc. 143 (1996) 2204.
[15] D.H. Jang, S.M. Oh, J. Electrochem. Soc. 144 (1997) 3342.

[16] D.H. Jang, S.M. Oh, Electrochim. Acta 43 (1998) 1023.
[17] R. Bittihn, R. Herr, D. Hoge, J. Power Sources 43/44 (1993) 223.
[18] G. Pistoia, A. Antonini, R. Rosati, C. Bellitto, G.M. Ingo, Chem. Mater. 9 (1997) 1443.
[19] L. Guohua, H. Ikuta, T. Uchida, M. Wakihara, J. Electrochem. Soc. 143 (1996) 178.
[20] K. Amine, H. Tukamoto, H. Yasuda, Y. Fujita, J. Electrochem. Soc. 143 (1996) 1595.
[21] Q. Zhong, A. Bonakdarpour, M. Zhang, Y. Gao, J.R. Dahn, J. Electrochem. Soc. 144 (1997) 205.
[22] Y. Ein Eli, W.F. Howard Jr., S.H. Lu, S. Mukerjee, J. McBreen, J.T. Vaughey, M.M. Thacheray, J. Electrochem. Soc. 145 (1998) 1238.
[23] H.-M. Zhang, Y. Teraoka, N. Yamazoe, Chem. Lett. (1987) 665.
[24] M.S.G. Baythoun, F.R. Sale, J. Mater. Sci. 17 (1982) 2757.
[25] G.H. Jeffery, J. Bassett, J. Mendham, R.C. Denney, in: Vogel's Textbook of Quantitative Chemical Analysis, 5th edn., Longman, New York, 1989, p. 584.
[26] A. Wattiaux, J.C. Grenier, M. Pouchard, P. Hagenmuller, J. Electrochem. Soc. 134 (1987) 1714.
[27] L.J. van der Pauw, Philips Research Reports 13 (1958) 1.
[28] H. Tukamoto, A.R. West, J. Electrochem. Soc. 144 (1997) 3164.
[29] V. Massarotti, D. Capsoni, M. Bini, G. Chiodelli, C.B. Azzoni, M.C. Mozzati, A. Paleari, J. Solid State Chem. 131 (1997) 94.
[30] W. Liu, K. Kowal, G.C. Farrington, J. Electrochem. Soc. 143 (1996) 3590.
[31] J.M. Tarascon, D. Guyomard, J. Electrochem. Soc. 138 (1991) 2864.